Accepted Manuscript

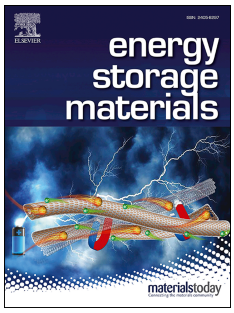

Surface engineering of commercial Ni foams for stable Li metal anodes

Xi Ke, Yaohua Liang, Lihui Ou, Haodong Liu, Yuanmao Chen, Wenli Wu, Yifeng Cheng, Zaiping Guo, Yanqing Lai, Ping Liu, Zhicong Shi

PII: S2405-8297(19)30082-0

DOI: https://doi.org/10.1016/j.ensm.2019.04.003

Reference: ENSM 698

To appear in: *Energy Storage Materials*

Received Date: 17 January 2019

Revised Date: 2 April 2019

Accepted Date: 3 April 2019

Please cite this article as: X. Ke, Y. Liang, L. Ou, H. Liu, Y. Chen, W. Wu, Y. Cheng, Z. Guo, Y. Lai, P. Liu, Z. Shi, Surface engineering of commercial Ni foams for stable Li metal anodes, *Energy Storage Materials* (2019), doi: https://doi.org/10.1016/j.ensm.2019.04.003.

Surface Engineering of Commercial Ni Foams for Stable Li Metal Anodes

Xi Ke[1], Yaohua Liang[1], Lihui Ou[2], Haodong Liu[3], Yuanmao Chen[1], Wenli Wu[1], Yifeng Cheng[1], Zaiping Guo[4], Yanqing Lai[5], Ping Liu[3*] and Zhicong Shi[1*]

[1] Guangzhou Key Laboratory of Low-dimensional Materials and Energy Storage Devices, School of Materials and Energy, Guangdong University of Technology, Guangzhou 510006, China

[2] College of Chemistry and Materials Engineering, Hunan University of Arts and Science, Changde 415000, China

[3] Department of Nanoengineering, University of California San Diego, La Jolla, San Diego, CA 92093, USA

[4] Institute for Superconducting and Electronic Materials, Australian Institute for Innovative Materials, University of Wollongong, Innovation Campus, North Wollongong, NSW 2500, Australia

[5] School of Metallurgy and Environment, Central South University, Changsha 410083, China

* Corresponding author:

piliu@eng.ucsd.edu (P. Liu), zhicong@gdut.edu.cn (Z. Shi)

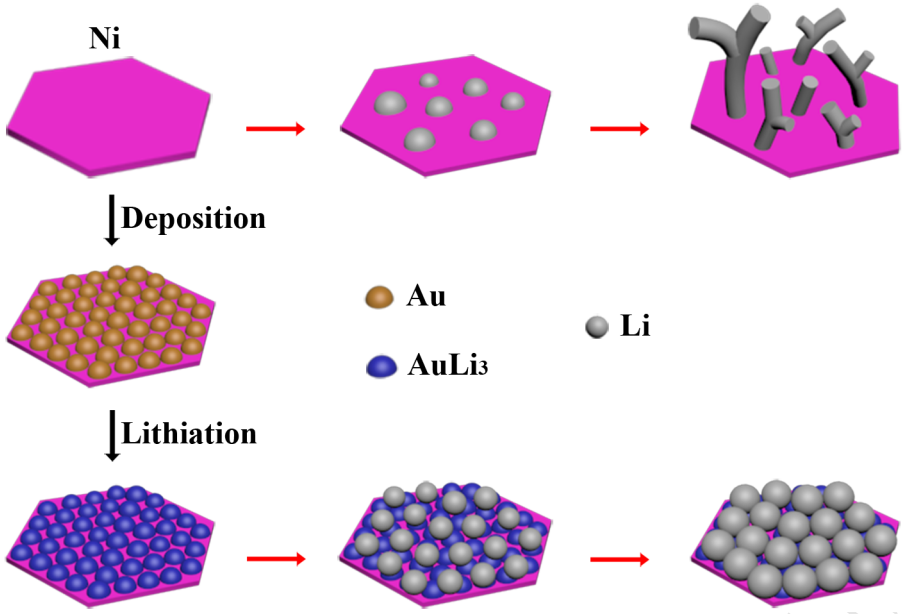

Surface Engineering of Commercial Ni Foams for Stable Li Metal Anodes

Abstract: The short life span of lithium metal anodes (LMAs) due to dendrite growth and low coulombic efficiency has been regarded as the bottleneck in developing next-generation high-energy-density lithium metal based secondary batteries. Employing three-dimensional (3D) current collectors is one approach to reduce the effective current density and delay dendrite growth. Commercial Ni foam, in spite of its high electronic conductivity and 3D topology, has not been considered for this application due to its low specific surface area and lithiophobic nature. In this study, we develop a surface engineering strategy to uniformly coat lithiophilic $AuLi_3$ particles on Ni foam skeletons through lithiation of electrodeposited gold nanoparticles. In comparison with the bare Ni foam, the $AuLi_3$@Ni foam is more lithiophilic, significantly lowering the nucleation energy barrier and enhancing the uniformity for Li deposition. Such a structure results in effective suppression of Li dendrite growth in the void space of the foam. As a result, the $AuLi_3$@Ni foam current collector based LMAs can run for 740 h without cell failure in a symmetric cell. Furthermore, the Li@($AuLi_3$@Ni foam)|$LiFePO_4$ full cell shows an excellent capacity retention of 43.8% with a high CE of 99.2% at 1 C for 500 cycles. This work further illustrates the critical importance of surface lithiophilicity in guiding lithium cycling and suggests engineering the skeleton surface of commercial metal foam current collectors is important to improve 3D structured LMAs.

Keywords: lithium metal anodes; current collectors; surface engineering; Ni foam; $AuLi_3$ particles

1. Introduction

Significant efforts have been devoted to developing lithium metal anodes (LMAs) for rechargeable Li batteries since the 1970s[1]. Besides their high capacity and low potentials, LMAs are requisite for Li-S and Li-O_2 systems[2, 3]. Unfortunately, the practical application of LMAs has been greatly impeded by low coulombic efficiency (CE) and Li dendrite growth and the serious associated safety hazards, which are intrinsically linked to the undesired reactions between the Li metal and the electrolyte during repeated Li plating/stripping[4]. There are a number of strategies that are proposed to mitigate these problems in LMAs, including adding electrolyte additives to generate a highly stable solid electrolyte interface (SEI) film[5, 6], constructing artificial SEI films to protect Li metal against liquid organic electrolytes[7-10], introducing insulating sheaths onto current collectors to homogenize electron/Li ion distribution at the anode/electrolyte interface[11, 12], modifying lithiophilic seeds on current collectors to induce uniform Li nucleation[13, 14], and embedding a stable host to mitigate volume change during Li plating/stripping cycling[15-17]. In accordance with the Sand's time model, which depicts an inversely proportional relationship between the time when Li dendrites begin to grow and the square of effective current density[18, 19], design of 3D, high-surface-area current collectors has also been introduced as an effective method for retarding Li dendrite growth by lowering the effective current density[20]. Based on this principle, a wide variety of

current collectors, such as graphene[21, 22], three-dimensional (3D) porous copper[23, 24], 3D hollow carbon fibers[25], and 3D graphitic carbon foam[26], have been examined.

Owing to the 3D interconnected porous architecture with excellent structural integrity and electrical conductivity, commercially available metal foams, such as Ni and Cu foams, have been widely employed as both the support substrate and current collector for various applications in electrocatalysis [27, 28], supercapacitors[29] and batteries[30]. Their low cost and demonstrated scalability make metal foams ideal for 3D Li hosts. However, the random macropores and the uneven transportation of Li ion flux on the metallic skeletons of these foams lead to the formation of dendritic and dead lithium. Consequently, they are regarded as an inferior type of 3D porous current collector for LMAs[23, 24]. Additionally, the intrinsic lithiophobicity of Ni and Cu surfaces increases Li nucleation overpotential, which could also induce Li dendrite growth[13]. Considering that the Li plating/stripping behavior is a surface-related process, engineering the surface properties of current collectors is important and effective for regulating Li electrodeposition behavior. Although there are some studies on the lithiophilic modification of various 3D current collectors including carbon fiber/foam[31-33] and copper/nickel foam[34-36], little attention was paid to investigate the structure evolution of the original lithiophilic layer after lithiation and its effect on the Li plating/stripping behavior.

In this study, we engineered the Ni foam surface by uniformly electrodepositing a layer of gold nanoparticles on the Ni skeletons, which was subsequently lithiated to

yield a layer of $AuLi_3$ particles modified onto Ni foam. This was used as a composite current collector in LMAs. The as-obtained current collector possesses very homogeneous surface properties with uniformly modified lithiophilic sites and therefore enables a homogeneous Li-ion flux distribution, leading to dendrite-free Li plating/stripping cycling. These features of the $AuLi_3$ modified Ni foam current collector enhance CE and prolong lifespan. In the Li/Li symmetric cells, the $AuLi_3$@Ni foam current collector based LMAs last for 740 h without cell failure. The Li@($AuLi_3$@Ni foam)/$LiFePO_4$ full cell shows an excellent capacity retention of 43.8% with a high CE of 99.2% at 1 C for 500 cycles.

2. Experimental section

2.1. Fabrication of gold-modified Ni foam (Au@Ni foam) composite

As-received commercial Ni foams (Changsha Lyrun Material Co., China) with a thickness of 0.5 mm and a porosity of 96.5 were cut into rectangular pieces with a size of 1×7 cm^2, which were firstly sequentially washed by acetone, ethanol and distilled water in a sonication bath for 15 min, and then immersed into a 1 mol L^{-1} HCl solution to remove the native oxide, and finally washed thoroughly with distilled water. The gold electrodeposition was conducted in a two-electrode setup using the as-pretreated Ni foam substrates as the working electrodes with a 1 cm^2 area exposed to the gold plating solution, and the Pt-modified Ti mesh as the counter electrode. The electrodeposition was carried out at a constant current density of 5 mA cm^{-2} for different time at 45 ºC.

2.2. Fabrication of $AuLi_3$@Ni foam current collectors

The Au@Ni foam composites were lithiated in CR2032-type coin cells, which were assembled in an argon-filled glove box with Au@Ni foam composites as the working electrodes, ceramic separators, and Li foils as the counter/reference electrodes. The electrolyte was composed of 1 mol L^{-1} lithium bis-(trifluoromethanesulfonyl)imide (LiTFSI) in 1,3-dioxolane/dimethoxyethane (DOL/DME, volume ratio 1:1) with 1% $LiNO_3$. The cells were firstly discharged to 0 V at a current density of 50 μA cm^{-2}, and then cycled between 0 and 0.1 V (*vs.* Li^+/Li) at 50 μA cm^{-2} for 5 cycles to stabilize the SEI.

2.3. Computational details

Calculations were performed in the framework of DFT on periodic super-cells using the generalized gradient approximation (GGA) of Perdew-Burke-Ernzerhof (PBE) functional[37] for exchange-correlation and ultrasoft pseudopotentials[38] for nuclei and core electrons. The Kohn-Sham orbitals were expanded in a plane-wave basis set with a kinetic energy cutoff of 30 Ry and the charge-density cutoff of 300 Ry. The Fermi-surface effects have been treated by the smearing technique of Methfessel and Paxton, using a smearing parameter[39] of 0.02 Ry. The PWSCF codes contained in the Quantum ESPRESSO distribution[40] were used to implement all calculations, while figures of the chemical structures were produced with the XCRYSDEN graphical package[41-43].

In all calculations, we used (2×2) five-layer fcc(111) slabs with theoretical equilibrium lattice constant to model the Ni(111) and Au(111) surfaces. Brillouin-zone

(BZ) integrations were performed with the special-point technique, using (4×4) uniformly shifted k-meshs for (2×2) slabs. Vacuum layers with thickness of 15 Å were added above the top layer of slabs in all cases. The atoms in the bottom two layers are fixed at the theoretical bulk positions, whereas the top three layers on (2×2) five-layer slabs are allowed to relax and all the other structural parameters have been optimized so as to minimize the total energy of the system. Structural optimization was performed until the Cartesian force components acting on each atom were brought below 10^{-3} Ry/Bohr and the total energy was converged to within 10^{-5} Ry with respect to structural optimization. The adsorption energies are calculated with the energies of the bare Ni(111) or Au(111) slab (E_{slab}) and the isolated Li atom (E_{Li}) as the references according to:

$$E_{ads} = E_{total} - E_{slab} - E_{Li}$$

where E_{total} refers to the total energies of the optimized slab/Li system. The more negative adsorption energy represents the stronger adsorption on the surface.

2.4. Characterization and electrochemical measurements

The current collectors were analyzed at room temperature by X-ray diffraction (XRD) using Rigaku D/max-2200/PC X-ray diffractometer with Cu Kα radiation at a wavelength of 0.1541 nm. The surface morphology of the samples was characterized by a field-emission scanning electron microscopy (FESEM, JEOL, JSM-6700F). In particular, for ex-situ measurements of LMAs, the coin cells were firstly disassembled in a glove box, the LMAs were then extracted and rinsed with DOL/DME solvents to get rid of residual electrolyte, and finally dried in the glove box. The LMAs were

transferred to the SEM via an air tight sample box.

The electrochemical performances of the LMAs were measured in CR2032-type coin cells which were assembled according to the above mentioned procedure. CEs were tested at different current densities and capacities with LAND battery testing system at room temperature. A certain amount of Li metal was plated onto the $AuLi_3$@Ni foam or bare Ni foam current collectors before charging to 0.1 V (*vs.* Li^+/Li) to strip Li metal at different current densities for each cycle, and an upper cut-off voltage of 0.1 V was set for cycling to prevent dealloying of Au-Li alloy. CEs were calculated as the ratio of the stripped to the plated amount of Li. For long-term galvanostatic charge/discharge cycling and full cell tests, 4 mAh cm^{-2} of Li was initially plated onto the current collectors at a current density of 0.5 mA cm^{-2}, and the cells were then repeatedly charged and discharged at different current densities and capacities. $LiFePO_4$ was used as the cathode material in the full cell with an areal capacity loading of 1.5 mAh cm^{-2}. Electrochemical impedance spectroscopy (EIS) measurements were performed using a ZIVE SP1 electrochemical workstation by applying a sine wave of 5 mV amplitude over a frequency range from 100 kHz to 0.01 Hz.

3. Results and discussion

Fig. 1 displays the surface morphology evolution of the current collectors at different stages during the fabrication. Specifically, the bare Ni foam was composed of 3D interconnected ligaments with a size of about 50-100 μm (Fig. 1A). The ligament consists of a large number of irregular microscale granules with relatively

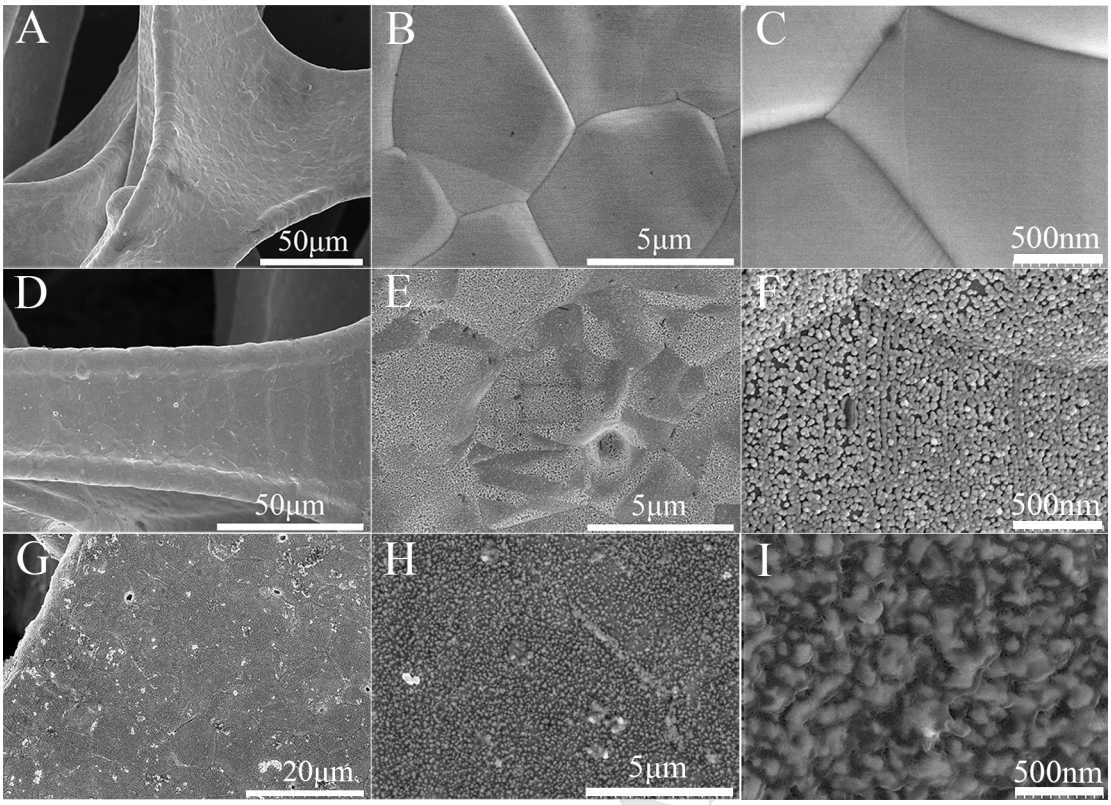

Figure 1. SEM images under different magnifications of pretreated Ni foam (A-C), gold nanoparticles coated Ni foam before (D-F) and after (G-I) lithiation.

smooth surfaces (Fig. 1B, C). After gold electrodeposition at a current density of 5 mA cm^{-2} for 200 s, a large quantity of dense gold nanoparticles was uniformly deposited and almost completely covered all of the Ni granule surfaces (Fig. 1D-F and Fig. S1A). The average size of gold nanoparticles is 65.6 ± 12.5 nm (Fig. S1B). It is noted that time of electrodeposition is an important parameter which affects both the surface morphology and the electrochemical performance of the current collector. The SEM images show that the surface of Ni foam skeleton was not completely covered by gold nanoparticles with a shorter electrodeposition time of 70 s (Fig. S2A, C), while a layer of loosely packed irregular gold nanoparticles formed on the surface of Ni foam skeleton with a longer electrodeposition time of 600 s (Fig. S2B, D). The

electrochemical measurements of the symmetric Li/Li cells also indicate that the LMAs based on the Ni foam modified with a gold electrodeposition time of 200 s, namely a nearly complete coverage of gold nanoparticles on the surface of Ni foam skeleton, exhibits best cycling performance (Fig. S3). Subsequently, the Au@Ni foam substrate were assembled into coin cells with Li foils. The cell was galvanostatically discharged to 0 V (*vs.* Li^+/Li) at a current density of 50 μA cm^{-2} (Fig. S4), through which gold first reacted with Li to form alloys and then the surface gold dissolved into Li[13]. The SEM images present a relatively smooth and homogeneous surface after the lithiation (Fig. 1G). A translucent thin coating is conformally wrapped on the gold nanoparticles (Fig. 1H, I), indicating the selective binding of Li with Au, which was verified by DFT calculations when determining the binding energies between an Au or Ni slab and a Li atom. The calculation results show that the Au(111) surface exhibits a much larger binding energy of -1.66 eV than the Ni(111) surface of -1.30 eV (Fig. 2A, B), revealing that the electrodeposited gold nanoparticles layer is much more lithiophilic than the bare Ni foam substrate.

XRD was employed to further characterize the crystalline phase of the Au@Ni foam and the lithiated Au@Ni foam. In order to enhance the intensity of the diffractive signal, the samples for XRD tests were prepared with a longer gold electrodeposition time of 60 min. The XRD pattern of the Au@Ni foam perfectly matches the standard patterns of pure Au (PDF, card no. 04-0784) and Ni (PDF, card no. 04-0850) (Fig. S5), confirming the deposition of gold on Ni foam substrate. For the fully lithiated Au@Ni foam, all the diffraction peaks are in good accordance with

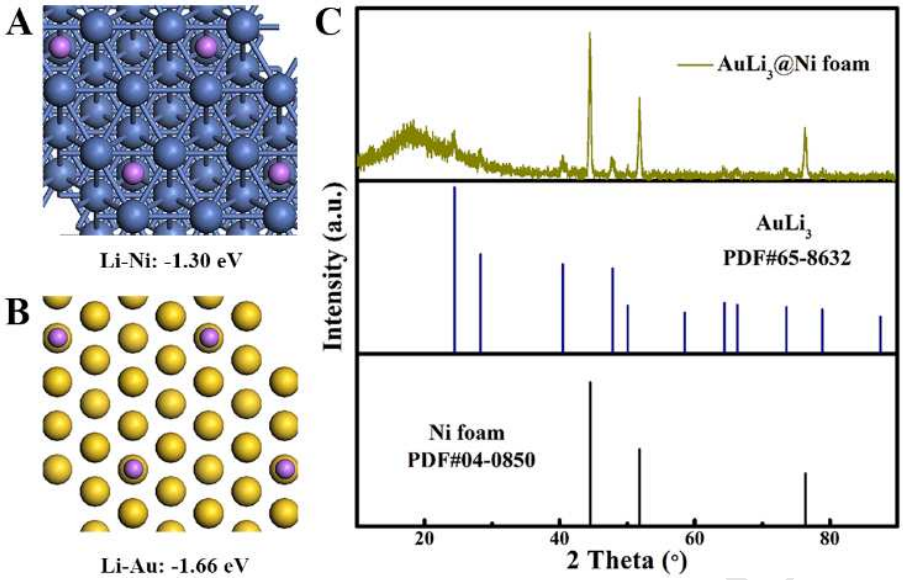

Figure 2. Calculated adsorption energies of a Li atom on Ni atoms (A) and Au atoms (B), XRD pattern of the $AuLi_3$@Ni foam (C).

the standard spectrum of Ni (PDF, card no. 04-0850) and $AuLi_3$ (PDF, card no. 65-8632) (Fig. 2C), except for the characteristic broad peak at 2θ = 17.9° from the polyimide tape that was used to protect the sample from air contamination. The XRD verifies that the alloy phase formed on the Au@Ni foam during the galvanostatic lithiation process is $AuLi_3$.

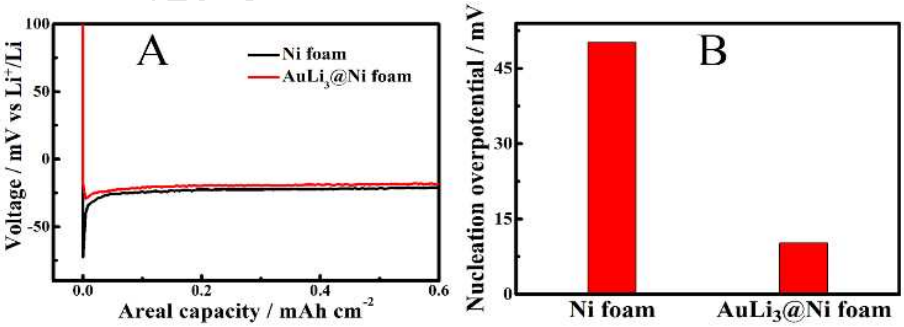

Figure 3. Voltage profiles of galvanostatic Li deposition on the bare Ni foam or $AuLi_3$@Ni foam substrates at a current density of 0.5 mA cm^{-2} (A), and the corresponding comparison of Li nucleation overpotentials (B).

Galvanostatic Li deposition on both bare Ni foam and $AuLi_3$@Ni foam substrates were conducted to study the Li deposition behaviors on different substrates. Fig. 3A shows that there is a very sharp voltage drop associated with the Li nucleation at the initial stage of the Li deposition on Ni foam, which is followed by a gradually steady voltage plateau. The difference between the flat part of the voltage plateau and the bottom of the voltage drop is used to define the nucleation overpotential. The Li nucleation overpotential of the bare Ni foam is 50.2 mV (Fig. 3B), which is utilized to overcome the energy barrier originated from the thermodynamic mismatch between Ni and Li. In comparison, the Li deposition on $AuLi_3$@Ni foam substrate exhibits a significantly smaller voltage drop at the beginning. The Li nucleation overpotential on $AuLi_3$@Ni foam substrate is only 10.2 mV (Fig. 3B). This significant reduction in nucleation overpotential therefore demonstrates that the surface engineering through the introduction of $AuLi_3$ particles on Ni foam substrate significantly improves the surface lithiophilicity of the substrate.

In order to evaluate the long term cycling stability of the $AuLi_3$@Ni foam in LMBs, both of the $AuLi_3$@Ni foam and bare Ni foam were cycled in a coin cell with Li foil as counter electrode. Fig. 4A-C show the surface morphology of the bare Ni foam current collectors after 100 cycles, the pores of the Ni foam are filled by Li infusion. Li dendrites severely grow on the Ni skeletons and inside the pores, which suggests that dendritic Li and dead Li are easily formed inside the macroscale pores of Ni foam, which is consistent with previous studies[23, 24]. Based on our previous work, it is possible that the growth of Li dendrites and dead Li is caused by the significant

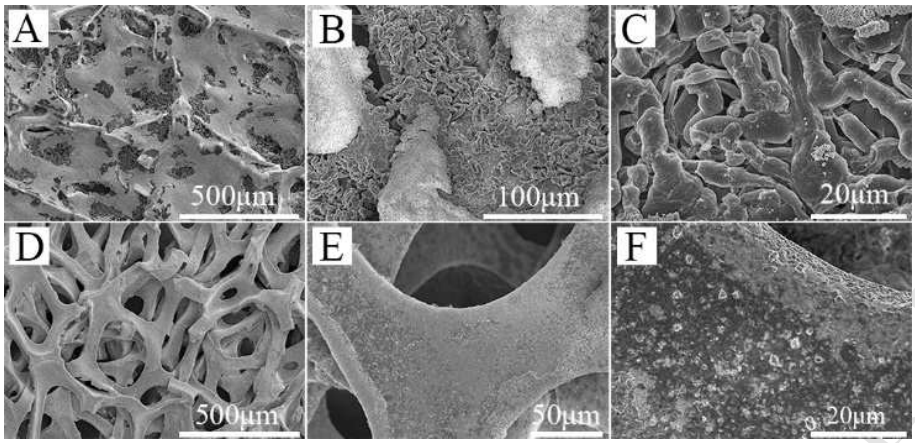

Figure 4. SEM images under different magnifications of the bare Ni foam (A-C) and $AuLi_3$@Ni foam (D-F) after 100 cycles of Li plating and stripping at a current density of 0.5 mA cm^{-2} with a capacity of 1 mAh cm^{-2} of Li metal.

difference of current density distribution between the ridges and flat regions on the Ni skeletons which leads to uneven Li ion flux[44]. Moreover, the Ni foam is intrinsically lithiophobic, resulting in a relatively large Li nucleation overpotential which accelerates Li dendrite growth. As depicted in Fig. S6, the molten Li droplet does not wet the bare Ni foam, while it spreads out and wets into the Au@Ni foam. Fig. 4D-F represent the morphology of the cycled $AuLi_3$@Ni foam current collectors. Fig. 4D demonstrates an outstanding morphological stability of $AuLi_3$@Ni foam without appearance of any Li dendrites and dead Li. The high magnification SEM images further illustrate a homogeneous and smooth skeleton surface (Fig. 4E, F), which is attributed to the homogeneous distribution of $AuLi_3$ particles that could induce uniform Li ion flux and facilitate Li nucleation. These results demonstrate that such a facile surface engineering strategy on commercial Ni foam is very effective at suppressing Li dendrites and dead Li growth.

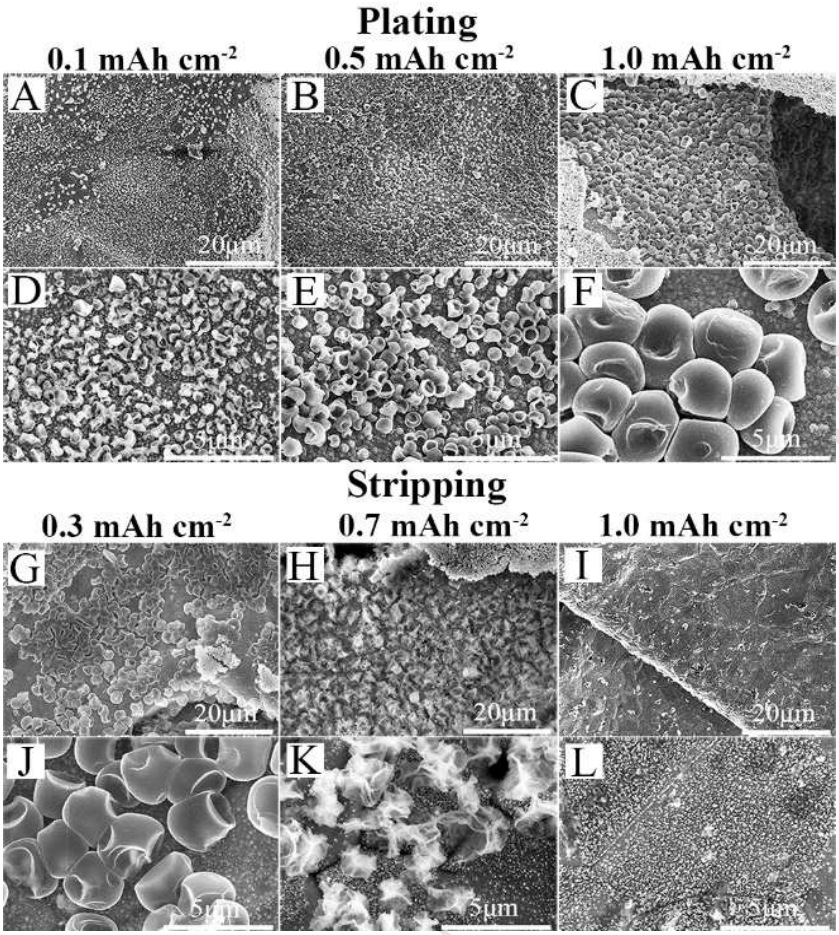

Figure 5. SEM images under different magnifications of lithium plating (A-F) and stripping (G-L) on the $AuLi_3$@Ni foam current collector with different capacities.

The Li deposition morphologies on the $AuLi_3$@Ni foam at different stages during Li plating/stripping were studied by SEM. The sample was prepared by depositing lithium at a current density of 0.5 mA cm^{-2} with a total capacity of 1 mAh cm^{-2}. Fig. 5A-C are the typical morphology of Li metal deposited with different capacities. A great number of spherical Li nuclei with relatively uniform size are homogeneously and densely packed on the skeleton surface. The corresponding higher magnification SEM images reveal that the sizes of these Li nuclei increase as the plating is going on (Fig. 5D-F). The dimples on these particles are probably generated by short exposure

to ambient conditions during sample transfer to the SEM chamber. The Li deposition on $AuLi_3$@Ni foam seems to be an instantaneous nucleation process followed by a continuous growth of the Li nuclei. During the Li stripping, the Li nuclei gradually collapse (Fig. 5G, H) and finally vanish on the skeleton (Fig. 5I). The skeleton emerges a nearly intact surface just like that of the original sample (Fig. 1G, H). The high magnification SEM images reveal that the morphology of the Li nuclei transitions from opaque spherical globules to translucent flaky flowers (Fig. 5J, K), and finally the densely and uniformly distributed $AuLi_3$ particles visibly appear on the skeleton (Fig. 5L). As a comparison, the Li deposition on the bare Ni foam exhibits a totally different trend (Fig. S7). During Li deposition, sparsely distributed Li nuclei form at a capacity of 0.1 mAh cm^{-2} (Fig. S7A), afterwards some nuclei preferentially grow and develop into mossy and filamentary Li at a capacity of 0.5 mAh cm^{-2} (Fig. S7B), which are further amplified at higher capacity (Fig. S7C). Although these dendritic structures can be partially stripped (Fig. S7D, E), there are still some residual Li dendrites after the stripping (Fig. S7F). The significantly improved capability for suppressing Li dendrites growth is attributed to the surface modification on Ni foam with $AuLi_3$ particles that not only effectively homogenize the surface's physico-chemical properties, but also greatly reduce the energy barrier for Li nucleation which yields a dendrite-free Li metal growth.

Based on the above results, the mechanism of the Li plating behavior on the bare Ni foam and $AuLi_3$@Ni foam current collectors are proposed (Scheme 1). On the bare Ni foam current collector, Li metal first nucleates sparsely and unevenly on the skeletons

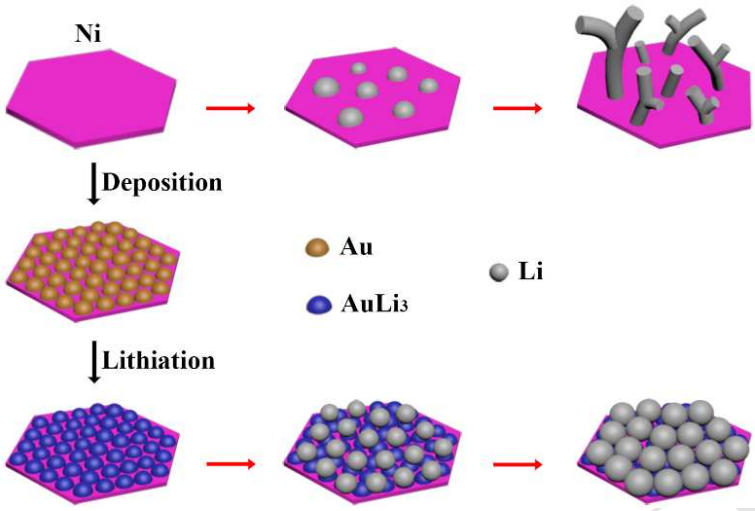

Scheme 1. Schematic diagram of the Li plating stages on the bare Ni foam (top) and $AuLi_3$@Ni foam (bottom) current collectors.

owing to the inhomogeneity on surfaces, which evolves into Li dendrites as the plating progresses. In comparison, Li metal uniformly nucleates on the $AuLi_3$ film due to the negligible nucleation energy barrier, and then these Li nuclei grow up homogeneously and merge into each other as the plating process continues, which gives a compact Li metal film on the preformed $AuLi_3$ layer.

The electrochemical performance of the $AuLi_3$@Ni foam current collector was evaluated by CE tests. Fig. 6A-B show voltage profiles of Li plating/stripping cycles on the Ni foam and $AuLi_3$@Ni foam current collectors, respectively, at a current density of 0.5 mA cm^{-2} with a capacity of 1 mAh cm^{-2}. The amount of stripped Li metal significantly decreased after 50 cycles for the bare Ni foam based electrode (Fig. 6A), while the discharge/charge curves for the $AuLi_3$@Ni foam based electrode remained unchanged after the first cycle (Fig. 6B). Fig. 6C shows that the $AuLi_3$@Ni foam-based electrode maintains a high CE of 98% over 100 cycles, while that of the

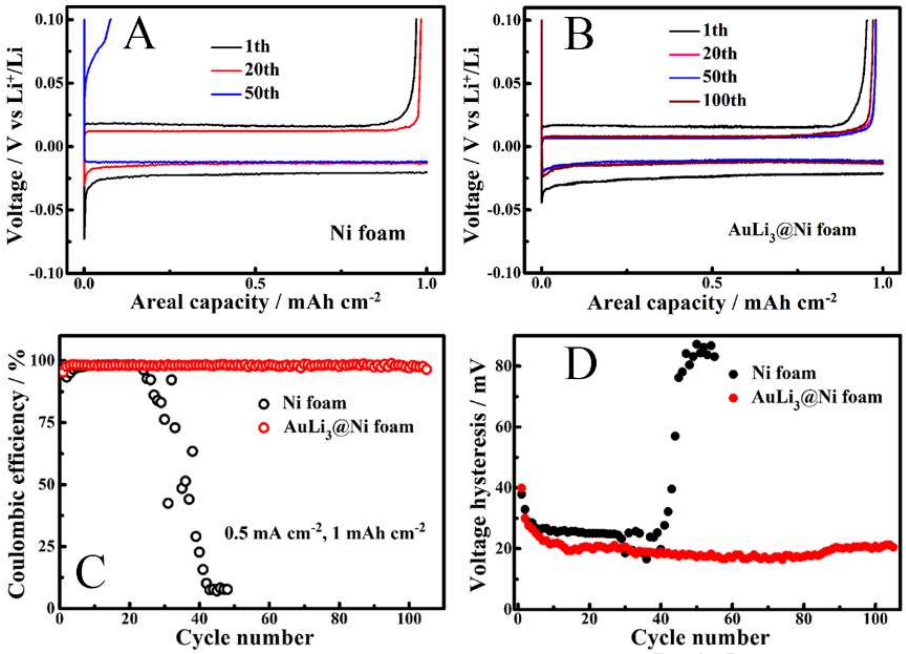

Figure 6. Voltage profiles (A, B), CEs (C) and voltage hysteresis (D) for Li metal plating/stripping cycles on the bare Ni foam and $AuLi_3$@Ni foam current collectors at a current density of 0.5 mA cm^{-2} with a capacity of 1 mAh cm^{-2} of Li metal.

bare Ni foam based electrode sharply drops to 7% after 50 cycles. At current densities of 1 and 2 mA cm^{-2}, the $AuLi_3$@Ni foam based electrode still maintains a high CE of 98% and 96% over 50 cycles, respectively, whereas the CEs of the bare Ni foam based electrode exhibit severe degradations within 10 cycles (Fig. S8). The rapid decrease of CEs for the Ni foam based electrode could be attributed to the uncontrollable growth of Li dendrites, causing continuous formation of SEI film and dead Li which largely consumes the active Li. The composition of the SEI films formed on the LMAs based on Ni foam and $AuLi_3$@Ni foam were characterized by *ex-situ* X-ray photoelectron spectroscopy (XPS). It is shown in Fig. S9 that the SEI layers are composed of alkyllithium, lithium carbonate, and lithium fluoride after the initial Li plating. After 20 cycles, the composition of SEI on the $AuLi_3$@Ni foam

shows much less changes than that of the Ni foam, indicating that the SEI layer on the $AuLi_3$@Ni foam maintains stable during Li plating/stripping which results in the improvement on coulombic efficiency. Fig. 6D displays the corresponding voltage hysteresis of both electrodes. Due to the removal of the high resistance native oxide layer on the bare Ni foam and Li foil surfaces, the bare Ni foam based electrode starts to exhibit a decrease in the voltage hysteresis at the beginning of cycling. After 40 cycles, its voltage hysteresis rapidly increases above 40 mV as a result of the accumulation of non-conductive SEI film formation. On the contrary, the $AuLi_3$@Ni foam based electrode exhibits a relatively smaller voltage hysteresis below 40 mV at the beginning, and then it gradually declines and stabilizes below 22 mV during the remaining cycles. The smaller and much more stable voltage hysteresis for the $AuLi_3$@Ni foam based electrode benefits from the compact and uniform plating of Li metal into the 3D porous structure of the $AuLi_3$@Ni foam, which facilitates electrolyte diffusion inside the electrode for high ionic mobility as well as accommodating the electrode volume change during plating/stripping cycling. In addition, the surface lithiophilicity of the $AuLi_3$@Ni foam based electrode reduces the polarization. All of the above merits of the $AuLi_3$@Ni foam based electrode are beneficial for stabilizing the interface and suppressing Li dendrites growth, and consequently reduce the voltage hysteresis.

The high interfacial stability of the $AuLi_3$@Ni foam based electrode compared to the bare Ni foam based electrode has also been confirmed by EIS measurements. Fig. 7 shows the Nyquist plots of the two electrodes after different cycles. The semicircles

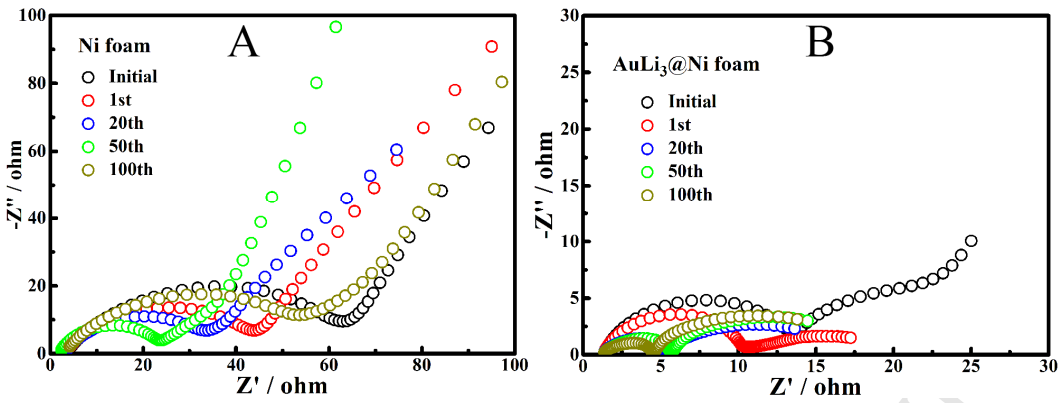

Figure 7. EIS for the Ni foam (A) and $AuLi_3$@Ni foam (B) based electrodes before cycling and after different cycles.

at high-frequency regions represent the interfacial resistance at the electrode/electrolyte interface, which also reflect the stability of the SEI film. The bare Ni foam based electrode shows a high interfacial resistance of 64 Ω before cycling, the resistance first declines to 23 Ω during the initial 50 cycles, and then increases to 55 Ω after 100 cycles (Fig. 7A), whereas the $AuLi_3$@Ni foam based electrode displays a low interfacial resistance of 14 Ω before cycling, and then it continuously reduces to only 4 Ω after 100 cycles (Fig. 7B). The initial decrease of the interfacial resistance could be ascribed to the decomposition of the native passivation layer on the electrode, while the significant increase of the resistance after longer cycling is caused by the Li dendrite growth leading to continuous formation of SEI layer which eventually increases the interfacial resistance. The smaller interfacial resistance further reveals that the $AuLi_3$@Ni foam based electrode possesses higher stability and provides better Li diffusion kinetics during Li plating/stripping cycling.

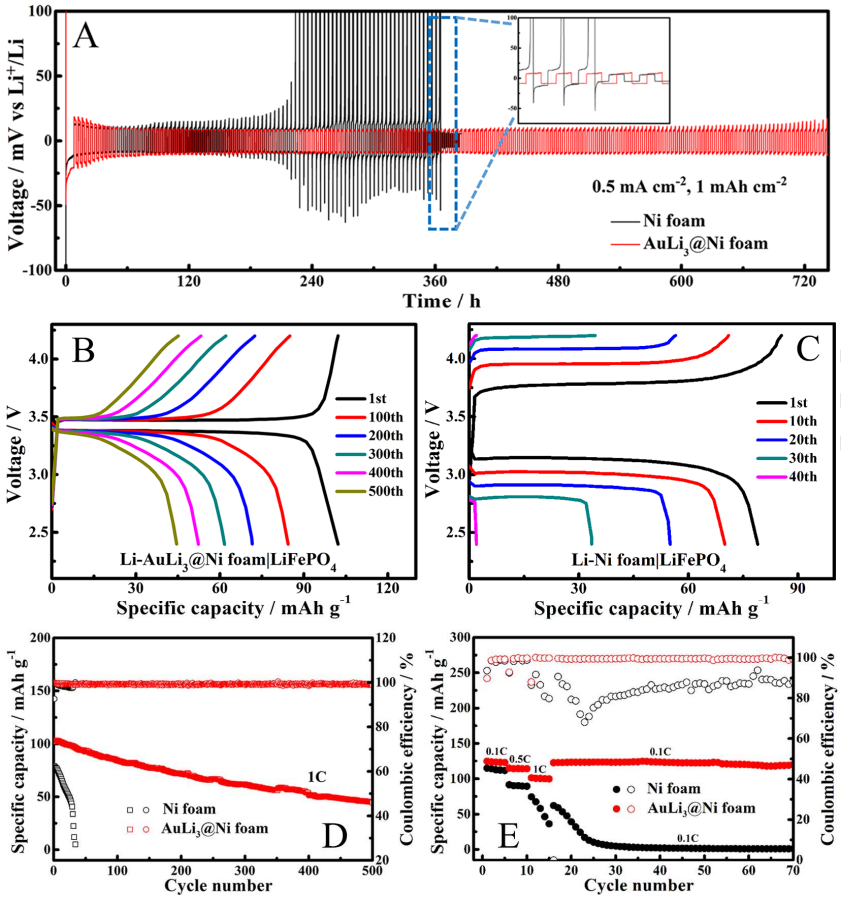

Figure 8. Voltage-time profiles of the Li plating/stripping cycles with a capacity of 1 mAh cm^{-2} of Li metal at a current density of 0.5 mA cm^{-2} in symmetric Li/Li@Ni foam and Li/Li@($AuLi_3$@Ni foam) cells (A), voltage-capacity profiles of Li-$AuLi_3$@Ni foam|$LiFePO_4$ (B) and Li-Ni foam|$LiFePO_4$ (C) full cells, and the corresponding cycling performance of the LMAs with the bare Ni foam and $AuLi_3$@Ni foam current collectors in a full cell with a $LiFePO_4$ cathode at 1 C (D). Rate capability of the LMAs with the bare Ni foam and $AuLi_3$@Ni foam current collectors in a full cell with a $LiFePO_4$ cathode (E).

Furthermore, the long-term cycling stabilities of the two electrodes were examined by measuring symmetric Li/Li cells with a Li foil counter/reference electrode and a Ni

foam or $AuLi_3$@Ni foam electrode pre-deposited with 4 mAh cm^{-2} of Li metal as the working electrode. The voltage-time profile (Fig. 8A) of the bare Ni foam basedelectrode exhibits random voltage oscillations after cycling for 220 h, resulting from the uncontrollable formation of a SEI film, and then a sudden voltage drop appears after 365 h, indicating short circuit problems and cell failure. In contrast, the Li plating/stripping on the $AuLi_3$@Ni foam based electrode displays significantly improved cycling stability without notable voltage fluctuation. There is no sign of cell failure after cycling for 740 h, implying that Li dendrite growth has been effectively suppressed. At higher current densities of 1.0 and 2.0 mA cm^{-2}, the $AuLi_3$@Ni foam based electrode also displays a smaller and much more stable voltage hysteresis than the bare Ni foam based electrode (Fig. S10).

The $AuLi_3$@Ni foam current collector pre-deposited with 4 mAh cm^{-2} of Li metal was paired with $LiFePO_4$ to evaluate its potential practical application. Fig. 8B-D show the voltage and capacity profiles of the full cells with the $AuLi_3$@Ni foam and bare Ni foam electrodes at 1 C for 500 cycles. The full cell with $AuLi_3$@Ni foam shows excellent cycling performance, the reversible capacity of the cell maintains at 45.2 mAh g^{-1} after 500 cycles, which is 43.8% of its original capacity, with a high CE of 99.2%. However, the capacity of the cell with bare Ni foam based LMA rapidly decreases to 6.5 mAh g^{-1} after only 33 cycles, corresponding to a capacity retention of 8.2%, with an average CE of 98.2%. Fig. 8E compares the rate capability of the full cells between the $AuLi_3$@Ni foam and bare Ni foam electrodes. The reversible capacity of the $AuLi_3$@Ni foam based cell is 123.7, 114.5 and 100.5 mAh g^{-1},

compared to 113.2, 90.2 and 56.5 mAh g^{-1} of the Ni foam based cell, at 0.1, 0.5 and 1 C, respectively. Apparently, the $AuLi_3$@Ni foam based cell exhibits significantly higher reversible capacity than the Ni foam based cell, revealing the profound effect of $AuLi_3$ surface modification of Ni foam on rate capability of the full cells.

4. Conclusion

In summary, we have demonstrated a surface engineering strategy for commercially available Ni foam current collectors by uniformly coating a lithiophilic $AuLi_3$ layer. Compared to the bare Ni foam current collector, the $AuLi_3$@Ni foam current collector exhibits a homogeneous surface with significantly lower nucleation energy barrier for Li metal nucleation, which is beneficial for the homogeneous and dense nucleation and subsequent uniform growth of Li metal. This improvement in surface property effectively suppresses the growth of Li dendrites in the void space inside the foam, leading to excellent electrochemical performance of the LMAs. The cells with $AuLi_3$@Ni foam current collectors deliver enhanced CEs, and therefore presented more stable cycling performance when Li plating/stripping. The $AuLi_3$@Ni foam based LMAs can run for 740 h without cell failure in a symmetric Li/Li@($AuLi_3$@Ni foam) cell at a current density of 0.5 mA cm^{-2} with a capacity of 1 mAh cm^{-2}. In addition, the Li@($AuLi_3$@Ni foam)|$LiFePO_4$ full cell shows excellent capacity retention at 1 C for 500 cycles. This work provides an example of engineering the skeleton surface of the commercially available metallic foam current collectors in order to effectively improve their electrochemical performance in LMAs for potential use in next-generation high-energy-density LMBs.

Supporting Information

Additional SEM, XRD characterizations, and additional electrochemical tests.

Notes

The authors declare no competing financial interest.

Acknowledgments

The research was supported by the National Key R&D Program of China (2018YFB0104202).

References

[1] M.S. Whittingham, History, evolution, and future status of energy storage, Proc. IEEE 100 (2012) 1518-1534.

[2] X.B. Cheng, R. Zhang, C.Z. Zhao, Q. Zhang, Toward safe lithium metal anode in rechargeable batteries: a review, Chem. Rev. 117 (2017) 10403-10473.

[3] W. Xu, J.L. Wang, F. Ding, X.L. Chen, E. Nasybutin, Y.H. Zhang, J.G. Zhang, Lithium metal anodes for rechargeable batteries, Energy Environ. Sci. 7 (2014) 513-537.

[4] D. Aurbach, E. Zinigrad, Y. Cohen, H. Teller, A short review of failure mechanisms of lithium metal and lithiated graphite anodes in liquid electrolyte solutions, Solid State Ionics 148 (2002) 405-416.

[5] Y.Y. Lu, Z.Y. Tu, L.A. Archer, Stable lithium electrodeposition in liquid and

nanoporous solid electrolytes, Nat. Mater. 13 (2014) 961-969.

[6] J.M. Zheng, M.H. Engelhard, D.H. Mei, S.H. Jiao, B.J. Polzin, J.G. Zhang, W. Xu, Electrolyte additive enabled fast charging and stable cycling lithium metal batteries, Nat. Energy, 2 (2017) 17012.

[7] G.Y. Zheng, S.W. Lee, Z. Liang, H.W. Lee, K. Yan, H.B. Yao, H.T. Wang, W.Y. Li, S. Chu, Y. Cui, Interconnected hollow carbon nanospheres for stable lithium metal anodes, Nat. Nanotechnol. 9 (2014) 618-623.

[8] N.W. Li, Y.X. Yin, C.P. Yang, Y.G. Guo, An artificial solid electrolyte interphase layer for stable lithium metal anodes, Adv. Mater. 28 (2016) 1853-1858.

[9] H.D. Liu, H.Y. Zhou, B.-S. Lee, X. Xing, M. Gonzalez, P. Liu, Suppressing lithium dendrite growth with a single-component coating, ACS Appl. Mater. Interfaces 9 (2017) 30635-30642.

[10] H.D. Liu, X.F. Wang, H.Y. Zhou, H.-D. Lim, X. Xing, Q.Z. Yan, Y.S. Meng, P. Liu, Structure and solution dynamics of lithium methyl carbonate as a protective layer for lithium metal, ACS Appl. Energy Mater. 1 (2018) 1864-1869.

[11] X.B. Cheng, T.Z. Hou, R. Zhang, H.J. Peng, C.Z. Zhao, J.Q. Huang, Q. Zhang, Dendrite-free lithium deposition induced by uniformly distributed lithium ions for efficient lithium metal batteries, Adv. Mater. 28 (2016) 2888-2895.

[12] T.T. Zuo, Y.X. Yin, S.H. Wang, P.F. Wang, X.N. Yang, J. Liu, C.P. Yang, Y.G. Guo, Trapping lithium into hollow silica microspheres with a carbon nanotube core for dendrite-free lithium metal anodes, Nano Lett. 18 (2018) 297-301.

[13] K. Yan, Z.D. Lu, H.W. Lee, F. Xiong, P.C. Hsu, Y.Z. Li, J. Zhao, S. Chu, Y. Cui,

Selective deposition and stable encapsulation of lithium through heterogeneous seeded growth, Nat. Energy, 1 (2016) 16010.

[14] C.P. Yang, Y.G. Yao, S.M. He, H. Xie, E. Hitz, L.B. Hu, Ultrafine silver nanoparticles for seeded lithium deposition toward stable lithium metal anode, Adv. Mater. 29 (2017) 1702714.

[15] Z. Liang, D.C. Lin, J. Zhao, Z.D. Lu, Y.Y. Liu, C. Liu, Y.Y. Lu, H.T. Wang, K. Yan, X.Y. Tao, Y. Cui, Composite lithium metal anode by melt infusion of lithium into a 3D conducting scaffold with lithiophilic coating, Proc. Natl. Acad. Sci. U.S.A. 113 (2016) 2862-2867.

[16] D.C. Lin, Y.Y. Liu, Z. Liang, H.W. Lee, J. Sun, H.T. Wang, K. Yan, J. Xie, Y. Cui, Layered reduced graphene oxide with nanoscale interlayer gaps as a stable host for lithium metal anodes, Nat. Nanotechnol. 11 (2016) 626-632.

[17] Y.Y. Liu, D.C. Lin, Z. Liang, J. Zhao, K. Yan, Y. Cui, Lithium-coated polymeric matrix as a minimum volume-change and dendrite-free lithium metal anode, Nat. Commun. 7 (2016) 10992.

[18] C. Brissot, M. Rosso, J.N. Chazalviel, P. Baudry, S. Lascaud, In situ study of dendritic growth in lithium/PEO-salt/lithium cells, Electrochim. Acta 43 (1998) 1569-1574.

[19] M. Rosso, T. Gobron, C. Brissot, J.N. Chazalviel, S. Lascaud, Onset of dendritic growth in lithium/polymer cells, J. Power Sources, 97-8 (2001) 804-806.

[20] L.Y. Qi, L.R. Shang, X. Chen, L.H. Ye, W.X. Zhang, P.J. Feng, W. Zou, N.Z. Cao, H.H. Zhou, D.A. Weitz, X. Li, A versatile strategy to fabricate 3D conductive

frameworks for lithium metal anodes, Adv. Mater. Interfaces, 5 (2018) 1800807.

[21] R. Zhang, X.B. Cheng, C.Z. Zhao, H.J. Peng, J.L. Shi, J.Q. Huang, J.F. Wang, F. Wei, Q. Zhang, Conductive nanostructured scaffolds render low local current density to inhibit lithium dendrite growth, Adv. Mater. 28 (2016) 2155-2162.

[22] A.R.O. Raji, R.V. Salvatierra, N.D. Kim, X.J. Fan, Y.L. Li, G.A.L. Silva, J.W. Sha, J.M. Tour, Lithium batteries with nearly maximum metal storage, ACS Nano 11 (2017) 6362-6369.

[23] C.P. Yang, Y.X. Yin, S.F. Zhang, N.W. Li, Y.G. Guo, Accommodating lithium into 3D current collectors with a submicron skeleton towards long-life lithium metal anodes, Nat. Commun. 6 (2015) 8058.

[24] Q.B. Yun, Y.B. He, W. Lv, Y. Zhao, B.H. Li, F.Y. Kang, Q.H. Yang, Chemical dealloying derived 3D porous current collector for Li metal anodes, Adv. Mater. 28 (2016) 6932-6939.

[25] L. Liu, Y.X. Yin, J.Y. Li, N.W. Li, X.X. Zeng, H. Ye, Y.G. Guo, L.J. Wan, Free-standing hollow carbon fibers as high-capacity containers for stable lithium metal anodes, Joule, 1 (2017) 563-575.

[26] L. Liu, Y.X. Yin, J.Y. Li, S.H. Wang, Y.G. Guo, L.J. Wan, Uniform lithium nucleation/growth induced by lightweight nitrogen-doped graphitic carbon foams for high-performance lithium metal anodes, Adv. Mater. 30 (2018) 1706216.

[27] W.G. Xi, G. Yan, Z.L. Lang, Y.Y. Ma, H.Q. Tan, H.T. Zhu, Y.H. Wang, Y.G. Li, Oxygen-doped nickel iron phosphide nanocube arrays grown on Ni foam for oxygen evolution electrocatalysis, Small 14 (2018) 1802204.

[28] D. Wu, Y.C. Wei, X. Ren, X.Q. Ji, Y.W. Liu, X.D. Guo, Z. Liu, A.M. Asiri, Q. Wei, X.P. Sun, $Co(OH)_2$ nanoparticle-encapsulating conductive nanowires array: room-temperature electrochemical preparation for high-performance water oxidation electrocatalysis, Adv. Mater. 30 (2018) 1705366.

[29] Z.C. Pan, Y.C. Jiang, P.Y. Yang, Z.Y. Wu, W.C. Tian, L. Liu, Y. Song, Q.F. Gu, D.L. Sun, L.F. Hu, In situ growth of layered bimetallic ZnCo hydroxide nanosheets for high-performance all-solid-state pseudocapacitor, ACS Nano 12 (2018) 2968-2979.

[30] X.W. Mu, Q.H. Wen, G. Ou, Y.M. Du, P. He, M.L. Zhong, H. Zhu, H. Wu, S.X. Yang, Y.J. Liu, B.J. Li, X.P. Zhang, H.S. Zhou, A current collector covering nanostructured villous oxygen-deficient NiO fabricated by rapid laser-scan for Li-O_2 batteries, Nano Energy, 51 (2018) 83-90.

[31] R. Zhang, X. Chen, X. Shen, X.Q. Zhang, X.R. Chen, X.B. Cheng, C. Yan, C.Z. Zhao, Q. Zhang, Coralloid carbon fiber-based composite lithium anode for robust lithium metal batteries, Joule, 2 (2018) 764-777.

[32] L. Liu, Y.X. Yin, J.Y. Li, S.H. Wang, Y.G. Guo, L.J. Wan, Uniform lithium nucleation/growth induced by lightweight nitrogen-doped graphitic carbon foams for high-performance lithium metal anodes, Adv. Mater., 30 (2018) 1706216.

[33] S.F. Liu, X.H. Xia, Z.J. Yao, J.B. Wu, L.Y. Zhang, S.J. Deng, C.G. Zhou, S.H. Shen, X.L. Wang, J.P. Tu, Straw-brick-like carbon fiber cloth/lithium composite electrode as an advanced lithium metal anode, Small Methods, 2 (2018) 1800035.

[34] L.G. Qin, H. Xu, D. Wang, J.F. Zhu, J. Chen, W. Zhang, P.G. Zhang, Y. Zhang,

W.B. Tian, Z.M. Sun, Fabrication of lithiophilic copper foam with interfacial modulation toward high-rate lithium metal anodes, ACS Appl. Mater. Interfaces, 10 (2018) 27764-27770.

[35] S.L. Wu, Z.Y. Zhang, M.H. Lan, S.R. Yang, J.Y. Cheng, J.J. Cai, J.H. Shen, Y. Zhu, K.L. Zhang, W.J. Zhang, Lithiophilic Cu-CuO-Ni hybrid structure: advanced current collectors toward stable lithium metal anodes, Adv. Mater., 30 (2018) 1705830.

[36] X.Y. Yue, W.W. Wang, Q.C. Wang, J.K. Meng, Z.Q. Zhang, X.J. Wu, X.Q. Yang, Y.N. Zhou, CoO nanofiber decorated nickel foams as lithium dendrite suppressing host skeletons for high energy lithium metal batteries, Energy Storage Mater., 14 (2018) 335-344.

[37] J.P. Perdew, K. Burke, M. Ernzerhof, Generalized gradient approximation made simple, Phys. Rev. Lett. 77 (1996) 3865-3868.

[38] D. Vanderbilt, Soft self-consistent pseudopotentials in a generalized eigenvalue formalism, Phys. Rev. B 41 (1990) 7892-7895.

[39] M. Methfessel, A.T. Paxton, High-precision sampling for Brillouin-zone integration in metals, Phys. Rev. B 40 (1989) 3616-3621.

[40] S. Baroni, A. Dal Corso, S. de Gironcoli, P. Giannozzi, http://www.quantum-espresso.org/, 2001.

[41] A. Kokalj, XCrySDen - a new program for displaying crystalline structures and electron densities, J. Mol. Graph. Model. 17 (1999) 176-179.

[42] A. Kokalj, M. Causa, Proceedings of high performance graphics systems and

applications European workshop, CINECA-Interuniversity Consortium, Bologna, Italy, 2000.

[43] A. Kokalj, M. Causa, http://www.xcrysden.org/, 2015.

[44] X. Ke, Y.F. Cheng, J. Liu, L.Y. Liu, N.G. Wang, J.P. Liu, C.Y. Zhi, Z.C. Shi, Z.P. Guo, Hierarchically bicontinuous porous copper as advanced 3D skeleton for stable lithium storage, ACS Appl. Mater. Interfaces 10 (2018) 13552-13561.